Biochimie 95 (2013) 1127–1135

Contents lists available at SciVerse ScienceDirect

Biochimie

journal homepage: www.elsevier.com/locate/biochi

Research paper

# Picosecond-resolved solvent reorganization and energy transfer in biological and model cavities

Subrata Batabyal, Tanumoy Mondol, Samir Kumar Pal*

*Department of Chemical, Biological & Macromolecular Sciences, S.N. Bose National Centre for Basic Sciences, Block JD, Sector III, Salt Lake, Kolkata 700 098, India*

ARTICLE INFO

*Article history:*
Received 2 November 2012
Accepted 21 December 2012
Available online 31 January 2013

*Keywords:*
Covalent fluorescent probe tagging
Water dynamics in cavities
Förster resonance energy transfer
Arrhenius type activation energy barrier
Energy barrier for viscous flow

ABSTRACT

Water molecules in hydrophobic biological cleft/cavities are of contemporary interest for the biomolecular structure and molecular recognition of hydrophobic ligands/drugs. Here, we have explored picosecond-resolved solvation dynamics of water molecules and associated polar amino acids in the hydrophobic cleft around Cys-34 position of Endogenous Serum Albumin (ESA). While site selective acrylodan labeling to Cys-34 allows us to probe solvation in the cleft, Förster resonance energy transfer (FRET) from intrinsic fluorescent amino acid Trp 214 to the extrinsic acrylodan probes structural integrity of the protein in our experimental condition. Temperature dependent solvation in the cleft clearly shows that the dynamics follows Arrhenius type behavior up to 60 °C, after which a major structural perturbation of the protein is evident. We have also monitored polarization gated dynamics of the acrylodan probe and FRET from Trp 214 to acrylodan at various temperatures. The dynamical behavior of the immediate environments around the probe acrylodan in the cleft has been compared with a model biomimetic cavity of a reverse micelle ($w_0 = 5$). Using same fluorescent probe of acrylodan, we have checked the structural integrity of the model cavity at various temperatures using picosecond-resolved FRET from Trp to acrylodan in the cavity. We have also estimated possible distribution of donor-acceptor distances in the protein and reverse micelles. Our studies reveal that the energetics of the water molecules in the biological cleft is comparable to that in the model cavity indicating a transition from bound state to quasibound state, closely consistent with a recent MD simulation study.



## 1. Introduction

The hydrophobic effect – the interaction of waters with nonpolar molecules – is very crucial in various fields of scientific research and most important in biomolecular structure and function [1]. Particularly, structure and energetics of water molecules in the hydrophobic cavity/cleft of protein trigger a number of research works in the field of experimental biophysics [2–6]. In most of the time "disordered" water molecules in hydrophobic protein cavities are essentially missed in X-ray crystallographic studies, however, clearly revealed in NMR structural studies [7]. From a number of recent experiments, it is an accepted fact that dynamical behavior of water molecules in hydrophobic protein cavities is not unique, rather very much case specific and depends on the structural (slower) [3] and functional (faster) [5] requirements of the protein. For example, due to substantial negative free energy generated by high enthalpy and low entropy factors, water molecules present within the substrate binding cavity of α-chymotrypsin are expelled easily upon ligand binding [8]. In many proteins, nonpolar cavities are often located at or near the active site and are thought to be involved in the uptake, transfer, and release of both nonpolar and polar molecules [9]. One of such examples include the presence of a cleft around Cys-34 (Fig. 1) in the domain I of endogenous serum albumin (ESA), which is reported to be responsible for the binding of an anticancer drug doxorubicin [10]. The X-ray structure of the native protein reveals that Cys-34 residing in a hydrophobic crevice that is ~10–12 Å deep from the protein surface [10]. Site selective acrylodan labeling of Cys-34, offers unique opportunity to investigate the dynamics of water molecules in the cleft. In recent past, Zewail group has explored the hydration dynamics using site selective acrylodan probe at Cys-34 and correlated the dynamics with unfolding pathways of the protein [11]. As mentioned in a review of biological water [12], femtosecond dynamics essentially reveals rotational and inertial (roto-translational) motions of water molecules, however, complete diffusion of water molecules in the several hundred ps to ns time scales is expected to be beyond experimental time windows of the measurement.

* Corresponding author. Tel.: +91 33 2335 5705/6/7/8; fax: +91 33 2335 3477.
*E-mail address:* skpal@bose.res.in (S.K. Pal).

0300-9084/$ – see front matter © 2013 Elsevier Masson SAS. All rights reserved.
http://dx.doi.org/10.1016/j.biochi.2012.12.018

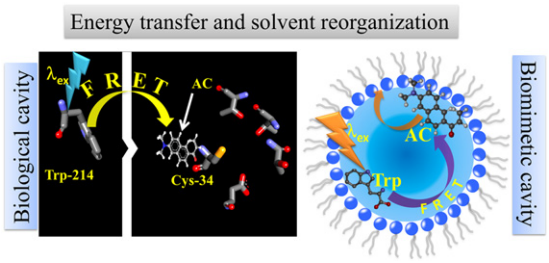


**Fig. 1.** The cavity region around Cys-34 in the protein is schematically presented (Left). Förster resonance energy transfer (FRET) from intrinsic tryptophan to acrylodan residing in the cavity attached to Cys-34 occurs upon excitation of tryptophan residue in the protein. In artificial biomimetic, AOT reverse micelle, the occurrence of FRET from tryptophan to acrylodan is schematically shown (Right).

In the present study, we have selectively labeled Cys-34 using thiol reactive probe acrylodan and probed the environmental dynamics with picosecond resolution in an experimental time window of several 10 s of nanoseconds. The hydrophobic crevice on the protein surface at Cys-34 is approximately 10–12 Å deep [10] and careful observation of the crystal structure [13] reveals the presence of 4–5 water molecules within 10 Å distance from Cys-34 residue. Temperature dependent solvation dynamics over wide range of physiologically relevant temperature region (10–70 °C) clearly indicates that dynamics is essentially due to the water molecules in the cleft and follows Arrhenius type behavior up to 60 °C, beyond which the structural integrity of the protein is not preserved [14]. Significant spectral overlap of the single tryptophan (Trp 214) with the site-selective probe acrylodan offers unique opportunity to apply FRET for the investigation of distance with molecular resolution between two specific sites at various temperatures, thus revealing the structural integrity of the protein in our experimental condition [15]. The distance distribution between donor and the acceptor in our experimental condition has also been investigated. Fluorescence anisotropy of acrylodan attached to Cys-34 at different temperatures reveal that physical motion of the probe is much slower than the reorganization of the immediate environments of the probe. In order to understand the importance of the water molecules in the solvation of acrylodan probe in the protein cleft, we have extended our studies on a nano-sized water pool of AOT (Aerosol-OT) reverse micelles (RMs) [16–18]. Similarity of the dynamics of the protein with that of RMs ($w_0 = 5$), indicates that the dynamics is essentially from water. A careful comparison of our dynamics in the above systems with those in MD simulation studies [19] reveals an interesting water dynamics in the cleft. The bound water molecules in the lower temperature undergo quasi-bound state, where the water molecules get immobilized by double or more hydrogen bond bridges and exhibit slower dynamics compared to free water molecules [20].

## 2. Material and methods

Bis (2-ethylhexyl) sulphosuccinate (AOT), Tryptophan, Endogenous Serum Albumin (ESA), and Phosphate buffer were obtained from Sigma. The fluorescent probe acrylodan was purchased from Molecular probe. The sample solutions were prepared in phosphate buffer (pH 7) using water from Millipore system. Preparation of ESA-acrylodan conjugate was done in the following way. Briefly, a stock solution containing 100 μM ESA was prepared in 0.1 M phosphate buffer pH 7.0. A minimum amount of concentrated acrylodan solution in dimethylformamide (~40 μl) was added to 5 ml of above solution to make final molar ratio of ESA to acrylodan to be 1:1. The mixture was stirred gently and maintained at room temperature for 2 h and then dialyzed at 4 °C against phosphate buffer. The dialysis buffer was changed at 12 h intervals for 3 days. AOT was dissolved in isooctane to a concentration of 100 mM, and then the calculated amount of water was injected into to form the reverse micelles (RMs) of desired hydration ($w_0 = 5$). For FRET study in RMs, the donor (tryptophan) concentration was 20 μM and the acceptor (acrylodan) was 130 μM. The steady-state absorption and emission spectra were measured with Shimadzu UV-2450 spectrophotometer and Jobin Yvon Fluoromax-3 fluorimeter, respectively.

Fluorescence transients were measured in a commercially available spectrophotometer (Life-Spec-ps) from Edinburgh Instrument, UK (excitation wavelength 375 nm, 70 ps instrument response function, (IRF)). Tryptophan was excited by the third harmonic laser beam (299 nm) of the 897 nm (0.5 nJ per pulse) using a mode-locked Ti-sapphire laser with an 80 MHz repetition rate (Tsunami, Spectra Physics), pumped by a 10 W Millennia (Spectra Physics) followed by a pulse-peaker (rate 8 MHz) and a third harmonic generator (Spectra-Physics, model 3980). The third harmonic beam was used for excitation of the sample inside the TCSPC instrument (instrument response function, IRF = 50 ps) and the second harmonic beam triggers the start pulse. The picosecond-resolved fluorescence transients were fitted with multi-exponential ($n$) function, $\sum_{i=1}^{n} A_i \exp\left(-\frac{t}{\tau_i}\right)$ where, $A_i$'s are weight percentages of the decay components with time constants of $\tau_i$. The average excited state lifetime is expressed by the equation $\tau = \sum_{i=1}^{n} A_i \tau_i$, when $\sum_{i=1}^{n} A_i = 1$.

The Förster distances of donor–acceptor pairs were calculated using the equation [21],

$$R_0 = 0.211 \times \left[\kappa^2 n^{-4} \Phi_D J(\lambda)\right]^{1/6} \text{ In } \left(\text{Å}\right) \quad (1)$$

where, $R_0$ is the distance between the donor and the acceptor at which the energy transfer efficiency is 50%, $\kappa^2$ is a factor describing the relative orientation in space of the transition dipoles of the donor and acceptor. The magnitude of $\kappa^2$ is assumed to be 0.66 for random orientation of donor and acceptor pair. The refractive index ($n$) of the medium is assumed to be 1.4 [21]. $J(\lambda)$, the overlap integral, which expresses the degree of spectral overlap between the donor emission and the acceptor absorption, is given by,

$$J(\lambda) = \frac{\int_0^\infty F_D(\lambda)\varepsilon_A(\lambda)\lambda^4 \mathrm{d}\lambda}{\int_0^\infty F_D(\lambda)\mathrm{d}\lambda} \quad (2)$$

where, $F_D(\lambda)$ is the fluorescence intensity of the donor in the wavelength range of $\lambda$ to $\lambda + \mathrm{d}\lambda$ and is dimensionless. $\varepsilon_A(\lambda)$ is the extinction coefficient (in $M^{-1}$ $cm^{-1}$) of the acceptor at $\lambda$. If $\lambda$ is in nm, then $J(\lambda)$ is in units of $M^{-1}$ $cm^{-1}$ $nm^4$. Once the value of $R_0$ is known, the donor–acceptor distance ($r$) can easily be calculated using the formula:

$$r^6 = \left[R_0^6(1-E)\right]/E \quad (3)$$

The efficiency of energy transfer ($E$) can be estimated from time-resolved studies by following equation:

$$E = 1 - \frac{\tau_{DA}}{\tau_D} \quad (4)$$

where $\tau_D$ and $\tau_{DA}$ are lifetimes of the donor in absence and in presence of the acceptor.

Distance distribution between donor and acceptor was estimated according to the procedure described in the literature [21]. The observed fluorescence transients of the donor molecules in absence of acceptor (acrylodan) in the protein and RMs were fitted using a nonlinear least-squares fitting procedure (software SCIENTIST) to the following function,

$$I_D(t) = \int_0^t E(t')P(t'-t)\mathrm{d}t' \tag{5}$$

which comprises the convolution of the instrument response function (IRF) (E(t)) with exponential ($P(t) = \sum_i \alpha_{Di}\exp(-t/\tau_{Di})$). The convolution of the distance distribution function $P(r)$ in the fluorescence transients of donor in presence of acceptor in the system under studies (protein and RMs) is estimated using the same software (SCIENTIST) in the following way.

The intensity decay of D–A pair, spaced at a distance $r$, is given by

$$I_{DA}(r,t) = \sum_i \alpha_{Di}\exp\left[-\frac{t}{\tau_{Di}} - \frac{t}{\tau_{Di}}\left(\frac{R_0}{r}\right)^6\right] \tag{6}$$

and the intensity decay of the sample considering P($r$) is given by

$$I_{DA}(t) = \int_{r=0}^{\infty} P(r)I_{DA}(r,t)\mathrm{d}r \tag{7}$$

where $P(r)$ consist of the following terms:

$$P(r) = \frac{1}{\sigma\sqrt{2\pi}}\exp\left[-\frac{1}{2}\left(\frac{\bar{r}-r}{\sigma}\right)^2\right] \tag{8}$$

In this equation $\bar{r}$ is the mean of the Gaussian with a standard deviation of $\sigma$. Usually distance distributions are described by the full width at half maxima. This half width is given by $hw = 2.354\sigma$.

To construct Time Resolved Emission Spectra (TRES), we followed the technique described in literature [21,22]. The time dependent fluorescence Stoke's shifts, as estimated from TRES, were used to construct the normalized spectral shift correlation function or the solvent correlation function, $C(t)$, defined as,

$$C(t) = \frac{\nu(t) - \nu(\infty)}{\nu(0) - \nu(\infty)} \tag{9}$$

where $\nu(0)$, $\nu(t)$, and $\nu(\infty)$ are the emission maxima (in $\mathrm{cm}^{-1}$) at time 0, $t$, and $\infty$, respectively. The $\nu(\infty)$ value corresponds to the emission frequency beyond which insignificant or no spectral shift is observed. The $C(t)$ function represents the temporal response of the solvent relaxation process, as occurs around the probe following its photo-excitation and the associated change in the dipole moment.

For anisotropy ($r(t)$) measurements, emission polarization was adjusted to be parallel or perpendicular to that of the excitation and anisotropy is defined as,

$$r(t) = \frac{[I_{\mathrm{para}} - I_{\mathrm{perp}}]}{[I_{\mathrm{para}} + 2\times I_{\mathrm{perp}}]} \tag{10}$$

The time-resolved anisotropy of a probe reveals the physical motion of the probe in a microenvironment. The time constants reflect rotational correlation time of the probe in the microenvironment. A fluorescent probe in a geometrical restriction can be well-represented in Wobbling-in-Cone model [23,24], where the rotational anisotropy is defined as:

$$r(t) = r_0\left(\beta e^{-t/\tau_{\mathrm{slow}}} + (1-\beta)e^{-t/\tau_{\mathrm{fast}}}\right) \tag{11}$$

According to this model $\tau_{\mathrm{slow}}$ and $\tau_{\mathrm{fast}}$ essentially represent the time constants for global tumbling motion of the host and lateral diffusion of the guest probe, respectively [23]. $\beta = S^2$ and $S$ is the generalized order parameter that describes the degree of restriction on the wobbling-in-cone orientational motion. The magnitude of $S$ is considered as a measure of the spatial restriction of the probe and can have a value from zero (for unrestricted rotation of the probe) to 1 (for completely restricted motion). The semicone angle $\theta_W$ is related to the ordered parameter as,

$$S = 0.5\times\cos\theta_W(1+\cos\theta_W) \tag{12}$$

$\theta_W$ can be calculated from the value of $S$ by using the following equation:

$$\theta_W = \cos^{-1}\left\{0.5\times\left([1+8\times S]^{1/2}-1\right)\right\} \tag{13}$$

The diffusion coefficient for wobbling motion $D_W$ can be obtained from the following relation,

$$D_W = \frac{1}{(1-S^2)\tau_W}\left[\frac{x^2(1+x)^2}{2(x-1)}\left\{\ln\left(\frac{1+x}{2}\right)+\left(\frac{1-x}{2}\right)\right\} + \frac{1-x}{24}\left(6+8x-x^2-12x^3-7x^4\right)\right] \tag{14}$$

Where $x = cos\theta_W$. The value of $\tau_W$, which represents the time constant for wobbling motion of the probe, can be obtained from the following equation:

$$\frac{1}{\tau_{\mathrm{fast}}} = \frac{1}{\tau_W} + \frac{1}{\tau_{\mathrm{slow}}} \tag{15}$$

The interfacial microviscosity ($\eta_m$) experienced by the probe at various temperatures [25], can also be estimated from the time-resolved fluorescence anisotropy using the modified Stokes–Einstein–Debye equation (SED) [26,27],

$$\tau_r = \frac{\eta_m V_h}{K_B T} \tag{16}$$

where $K_B$ is the Boltzmann constant, $T$ the absolute temperature. $\tau_r$ refers to the faster decay time in the anisotropy decay which describes the tumbling motion of the probe. Hydrodynamic volume of the probe ($V_h$) can be calculated as:

$$V_h = V_m f C \tag{17}$$

where $f$ is the shape factor ($f = 1$ for a spherical probe) and $C$ represents solute-solvent coupling constant ($C = 1$ for "stick" condition and $C < 1$ for "slip" condition) and $V_m$ the molecular volume of the probe [28]. In our case, molecular volume of acrylodan was estimated to be 222 Å$^3$. In case of $f = C = 1$, Eq. (16) reduces to the original simple SED equation [29],

$$\tau_r = \frac{\eta_m V_m}{K_B T} \tag{18}$$

## 3. Results and discussion

Fig. 2A depicts the fluorescence characteristics of acrylodan probe attached to Cys-34 residue of Endogenous Serum Albumin (ESA). As shown in the figure, the emission is blue shifted from 530 nm (in buffer) to 488 nm upon covalent attachment to Cys-34 residue in protein. As the fluorescence of acrylodan is very sensitive to the polarity of the medium [30], it can be used to probe the solvation dynamics in the surrounding environment [11]. With increasing temperature (10–70 °C), the emission of the probe in the protein is observed to be slightly blue shifted (Fig. 2A), which indicates that probe resides in hydrophobic cleft even at elevated temperatures. Fig. 2B reveals temperature dependent picosecond-resolved Förster resonance energy transfer (FRET) from intrinsic tryptophan of ESA to extrinsic fluorescent probe acrylodan. It is well documented that tryptophan and acrylodan serve as excellent FRET pair [31,32] as there is significant spectral overlap between tryptophan emission and acrylodan absorption spectrum. The FRET study confirms the location of the probe (Fig. 1) and also elucidates structural integrity of the protein at various temperatures (10–70 °C). As evident in the inset of Fig. 2B, at 10 °C, the lifetime of tryptophan is significantly quenched in acrylodan labeled ESA in comparison to unlabeled ESA. The lifetime quenching occurs due to the nonradiative energy transfer from tryptophan to acrylodan (FRET). From the observed FRET efficiency of 83% at 10 °C, the distance ($r$ = 36 Å) between tryptophan and acrylodan was estimated according to equation (3) and found to be in good agreement with the distance (~40 Å) between Cys-34 and Trp 214 as revealed from the X-ray crystal structure (PDB code: 2XSI [13]). At 10 °C, tryptophan in ESA has lifetime decay components of 0.18 ns (20%), 3.16 ns (25%) and 7.96 ns (55%) with average lifetime of 5.13 ns. In the acrylodan labeled ESA, the lifetime components of tryptophan becomes 0.10 ns (54%), 0.97 ns (33%) and 4.20 ns (13%) with average lifetime of 0.9 ns. With increasing temperature, lifetime of tryptophan in both labeled and unlabeled protein is affected due to the perturbation of the secondary structure of the protein. As shown in the inset of Fig. 2B, at 70 °C, the tryptophan lifetime becomes faster in both the cases and overall FRET efficiency is estimated to be 70%. The lifetime values of tryptophan under various conditions are summarized in Table 1. As shown in Fig. 2B, the temperature dependent energy transfer profile consists of three distinct regions, 10 °C–30 °C, 30 °C–60 °C and above 60 °C. The efficiency up to 30 °C sharply decreases from 82% to 72% and remains almost same up to 60 °C after which it starts to fall again. Around 60 °C, the protein structure is reported to be collapsed [14] which is well reflected in our temperature dependent FRET studies. The sharp change in the energy transfer efficiency with increase of temperature from 10 to 30 °C could be attributed to the different flexibilities of the protein domains (I, II and III) [11] at various thermal regions. However, the CD study [14] of thermal unfolding of the protein does not reveal any such specific pattern and requires further investigation to appropriately justify the behavior.

In order to exploit the local environmental dynamics around acrylodan attached to Cys-34 residue of ESA, wavelength dependent fluorescence transients of acrylodan in ESA were collected starting from lower (10 °C) to higher temperatures (70 °C). The

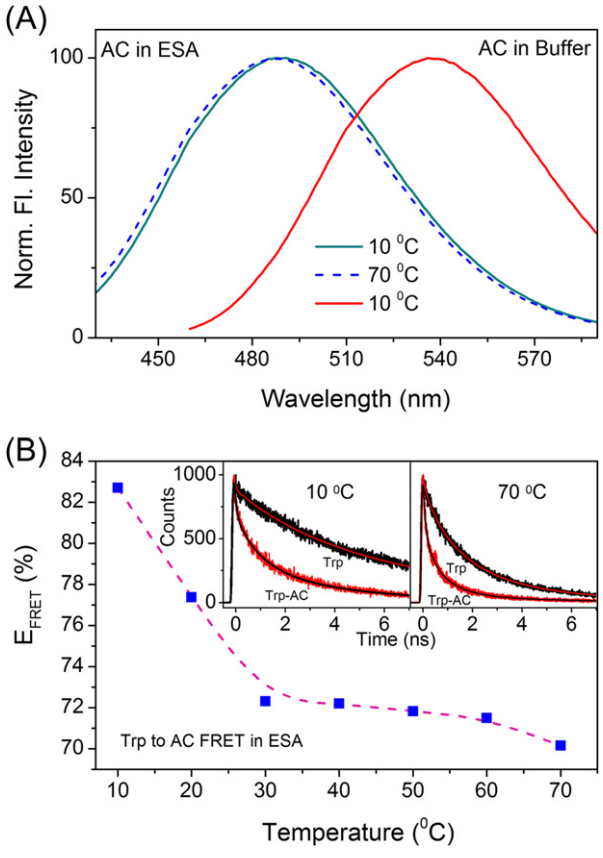


**Fig. 2.** (A) Represents the steady-state emission spectrum of acrylodan (AC) in buffer and in endogenous serum albumin (ESA). The emission of acrylodan is significantly blue shifted in protein. The dotted line indicates the emission spectrum of acrylodan in ESA at elevated temperature (70 °C). (B) The energy transfer efficiency from tryptophan to acrylodan in the protein at various temperatures was estimated as represented in the figure. The dotted line is the guide to the eye. The inset figures show the lifetime quenching of tryptophan (Trp) in presence of acrylodan (Trp-AC) at two representative temperatures in ESA protein. Tryptophan was excited at 299 nm and emission was collected at 350 nm.

**Table 1**
Fluorescence lifetimes ($\tau_i$), average fluorescence lifetimes $<\tau_{avg}>$, respective amplitudes (Amp %) and Förster resonance energy transfer (FRET) efficiency ($E_{FRET}$ %) from tryptophan (Trp) to acrylodan (AC) at different temperatures.

| Systems | Temperature (°C) | $\tau_1$ (ns) | $\tau_2$ (ns) | $\tau_3$ (ns) | $<\tau_{avg}>$ (ns) | $E_{FRET}$ (%) |
|---|---|---|---|---|---|---|
| FRET in ESA | | | | | | |
| Trp | 10 | 0.15 (20%) | 3.16 (25%) | 7.96 (55%) | 5.14 | 82.7 |
| Trp-AC | | 0.10 (55%) | 0.97(33%) | 4.19 (12%) | 0.89 | |
| Trp | 20 | 0.11 (20%) | 1.93(15%) | 6.99 (65%) | 4.88 | 77.3 |
| Trp-AC | | 0.08 (50%) | 0.87 (30%) | 3.79 (20%) | 1.10 | |
| Trp | 30 | 0.15 (17%) | 2.35 (21%) | 6.66 (62%) | 4.60 | 72.3 |
| Trp-AC | | 0.18 (47%) | 1.19 (32%) | 3.97 (21%) | 1.27 | |
| Trp | 40 | 0.10 (24%) | 2.56 (31%) | 6.51 (45%) | 3.77 | 73.7 |
| Trp-AC | | 0.11 (52%) | 1.02 (30%) | 3.73 (18%) | 0.99 | |
| Trp | 50 | 0.09 (25%) | 1.96 (25%) | 5.23 (50%) | 3.13 | 71.8 |
| Trp-AC | | 0.20 (54%) | 1.02 (33%) | 3.48 (13%) | 0.88 | |
| Trp | 60 | 0.17 (17%) | 1.72 (37%) | 4.43 (46%) | 2.69 | 71.9 |
| Trp-AC | | 0.14 (49%) | 0.78 (38%) | 3.15 (13%) | 0.75 | |
| Trp | 70 | 0.18 (28%) | 1.41 (46%) | 3.99 (26%) | 1.73 | 70.1 |
| Trp-AC | | 0.11 (65%) | 0.76 (28%) | 3.53 (07%) | 0.51 | |
| FRET in AOT RMs | | | | | | |
| Trp | 10 | 0.10 (20%) | 1.80 (30%) | 6.21 (50%) | 3.67 | 75.4 |
| Trp-AC | | 0.10 (54%) | 0.97 (33%) | 4.23 (13%) | 0.90 | |
| Trp | 20 | 0.11 (19%) | 1.81 (34%) | 6.19 (47%) | 3.52 | 74.9 |
| Trp-AC | | 0.11 (55%) | 0.85 (31%) | 4.22 (14%) | 0.88 | |
| Trp | 30 | 0.14 (18%) | 2.35 (21%) | 6.66 (61%) | 4.60 | 70.9 |
| Trp-AC | | 0.15 (47%) | 1.19 (33%) | 4.13 (20%) | 1.25 | |
| Trp | 40 | 0.10 (23%) | 2.32 (29%) | 5.52 (48%) | 3.29 | 66.4 |
| Trp-AC | | 0.12 (53%) | 1.25 (30%) | 4.11 (17%) | 1.10 | |
| Trp | 50 | 0.08 (25%) | 1.86 (28%) | 4.82 (47%) | 2.79 | 58.2 |
| Trp-AC | | 0.12 (51%) | 1.21(29%) | 3.88 (20%) | 1.16 | |
| Trp | 60 | 0.18 (28%) | 1.68 (46%) | 4.52 (26%) | 1.98 | 52.1 |
| Trp-AC | | 0.12 (53%) | 1.02 (31%) | 3.61 (16%) | 0.94 | |
| Trp | 70 | 0.18 (28%) | 1.65 (46%) | 4.21 (26%) | 1.86 | 48.5 |
| Trp-AC | | 0.12 (53%) | 1.02 (30%) | 3.64 (17%) | 0.96 | |

fluorescence transients collected at blue end, decay faster in comparison to the transients collected at the red end of the spectrum. Time-resolved emission spectra (TRES) were constructed from the fluorescence decay transients for different temperatures. As illustrated in Fig. 3A, at lower temperature (10 °C), the net spectral shift in TRES was estimated 1500 $cm^{-1}$ in 1 ns time window. The spectral shift decreases with increasing temperature and becomes 700 $cm^{-1}$ at 70 °C. The decrease in the spectral shift of 800 $cm^{-1}$, associated with faster solvation at elevated temperatures confirms that a considerable fraction of solvation is lost due to the transition of water molecules. Fig. 3B represents the solvation correlation function ($C(t)$) constructed for acrylodan probe attached to Cys-34 in ESA at various temperatures. The solvation correlation decay profiles were fitted to bi-exponential function to obtain water relaxation times and corresponding decay constants are tabulated in Table 2. The overall decrease of solvation correlation decay time up to certain temperature range (~60 °C) indicates that increase in temperature accelerates the solvation process leading to a decrease in water relaxation time. The observed temperature-induced acceleration of solvation dynamics of acrylodan in ESA is associated with the transition of water molecules with temperature, which in turn is governed by an Arrhenius type of activation energy barrier crossing model [33,34]. The activation energy barrier crossing model was applied in order to calculate the activation energy barrier ($E_a$) for water transition using the following relation [33],

$$\frac{1}{<\tau_{solv}>} = k_{bf} = A\ \exp\left(-\frac{E_a}{RT}\right) \quad (19)$$

where, $<\tau_{solv}>$ represents the average solvation time constant, $k_{bf}$ is the rate of water conversion, $A$ is the pre-exponential factor and $E_a$ is the corresponding activation energy for the transition process.

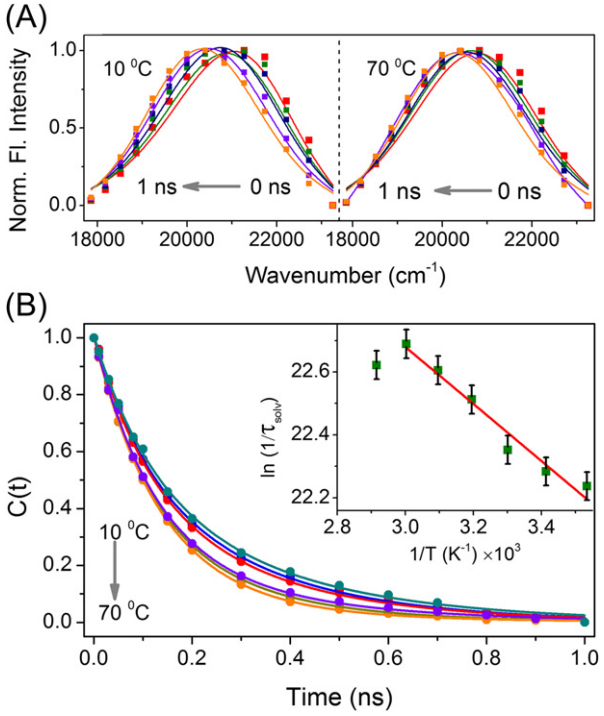


**Fig. 3.** (A) Depicts the constructed TRES for acrylodan attached to Cys-34 in endogenous serum albumin (ESA) at two different temperatures, 10 °C and 70 °C. (B) Solvation correlation decay profiles of acrylodan in ESA at various temperatures are plotted. Inset shows the plot of $1/\tau_{solv}$ against $1/T$ (the solid line is a fitting to the Arrhenius equation with 1% error bar).

**Table 2**
Solvation correlation data for acrylodan in ESA and AOT RMs at different temperature values.[a]

| Temperature (°C) | $a_1$ | $\tau_1$ (ns) | $a_2$ | $\tau_2$ (ns) | $<\tau_{solv}>$ | $E_a$ (kcal $mol^{-1}$) |
|---|---|---|---|---|---|---|
| Acrylodan in ESA | | | | | | 1.80 ± 0.1 |
| 10 | 0.39 | 0.30 | 0.60 | 0.28 | 0.25 | |
| 20 | 0.46 | 0.11 | 0.53 | 0.32 | 0.23 | |
| 30 | 0.50 | 0.11 | 0.50 | 0.29 | 0.20 | |
| 40 | 0.61 | 0.13 | 0.36 | 0.23 | 0.17 | |
| 50 | 0.68 | 0.11 | 0.31 | 0.25 | 0.15 | |
| 60 | 0.85 | 0.13 | 0.12 | 0.27 | 0.14 | |
| 70 | 0.72 | 0.14 | 0.28 | 0.18 | 0.15 | |
| Acrylodan in AOT RMs | | | | | | 1.90 ± 0.2 |
| 10 | 0.67 | 0.15 | 0.37 | 0.46 | 0.26 | |
| 20 | 0.68 | 0.15 | 0.38 | 0.46 | 0.26 | |
| 30 | 0.67 | 0.15 | 0.38 | 0.46 | 0.26 | |
| 40 | 0.65 | 0.15 | 0.36 | 0.43 | 0.25 | |
| 50 | 0.72 | 0.15 | 0.31 | 0.44 | 0.23 | |
| 60 | 0.80 | 0.14 | 0.23 | 0.46 | 0.21 | |
| 70 | 0.70 | 0.08 | 0.36 | 0.40 | 0.18 | |

[a] $\tau$ represents the solvent correlation time constant, a represents its relative weight. $\tau_{solv}$ is the average solvation correlation decay time.

Activation energy for water transitions was estimated from the slope of the plot of $\ln(1/\tau_{solv})$ against $1/T$. The activation energy ($E_a$) was found to be 1.80 ± 0.1 kcal $mol^{-1}$. It is well documented that transition of bound to the bulk-type water is associated with a higher energy barrier of 7–8 kcal $mol^{-1}$, which is much higher than our estimated value [35,36]. The activation energy barrier value is closely consisted with the transition of water from bound to quasibound state in the cavity around the probe attached to Cys-34 [20].

At this juncture, it is important to know the rotational flexibility of the probe acrylodan in the cavity in the experimental temperature range (10–70 °C). Fig. 4A represents the polarization gated time-resolved anisotropy decay of acrylodan attached to Cys-34 at two different temperatures. As evident from the Fig. 4A, at 10 °C, the anisotropy decay is much slower in comparison to that at 70 °C. The anisotropy decay collected at 10 °C consists of bi-exponential

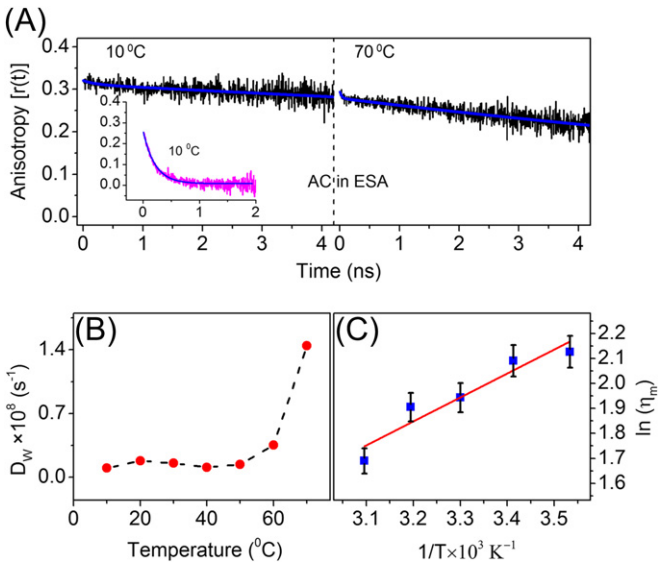


**Fig. 4.** (A) Temporal decays of rotational anisotropy at 10 °C and 70 °C of acrylodan (AC) covalently attached to Cys-34 are shown. Inset figure depicts the rotational anisotropy of acrylodan ($\tau_{rot}$ = 200 ps) in phosphate buffer (B) diffusion coefficient for wobbling motion ($D_W$) of AC in ESA at different temperatures. Dotted line is guide to eye. (C) Plot of $ln(\eta_m)$, $\eta_m$expressed in cP, against $1/T$ of AC in ESA with a linear fit (2% error bar included).

decay function having time constant of 60 ns (96%) and 0.50 ns (04%). The 60 ns component reveals the overall global motion of the protein molecule and is consistent with the reported value [14]. The shorter 0.5 ns component with insignificant weightage represents the rotational motion of the probe within its immediate microenvironment [14]. At elevated temperature of 70 °C, the anisotropy decay constants become 15 ns (93%) and 50 ps (7%). The average rotational time constants $\tau_{rot}$, were estimated at various temperatures and summarized in Table 3. To account for the effect of temperature on the rotational relaxation process of the probe in the protein cavity, the anisotropy decays were analyzed using the wobbling-in-cone model [24]. Fig. 4B represents the change of diffusion coefficient for wobbling motion ($D_W$) value with increasing temperature. The diffusion coefficient ($D_W$) values are of the same order of magnitude as reported in one of our earlier works on another probe in the protein [23]. The corresponding semicone angles ($\theta_W$) experienced by the acrylodan probe in different thermal regions are summarized in Table 3. The observation is consistent with higher lability of the probe AC in the protein cavity at elevated temperature. Fig. 4C represents the plot of microviscosity, experienced by the probe at different temperatures. The energy barrier ($E_n$) for the viscous flow can be obtained using the following equation by estimating the microviscosity ($\eta_m$) at different temperatures [37],

$$\eta_m = \eta_0 \exp\left(\frac{E_n}{RT}\right) \tag{20}$$

The energy barrier ($E_n$) for the viscous flow was estimated from the slope of the plot of $ln(\eta_m)$ against $1/T$. As shown in Fig. 4C, a good linear fit was obtained with an estimated $E_n$ value of 1.90 ± 0.2 kcal mol$^{-1}$. The good agreement between the energy barrier values ($E_n$ obtained from the rotational anisotropy study and $E_a$ value obtained from solvation dynamics study) is indicative of the interlinking of the two processes involved in the cavity. It has to be noted that, there prevails a possibility of interference bond rotation in the solvation dynamics [38]. In our case, the possibility of interference of bond rotation in the solvation dynamics, can be safely rule out as the solvation time scale ($\tau_{solv}$ = 230 ps) is much faster compared to the rotational flexibility of the probe ($\tau_{rot}$ = 500 ps) as observed with time-resolved anisotropy study.

In order to compare the dynamics and energetics of water molecules with that in a well-known model biomimetic cavity, similar experiments were carried out in AOT reverse micelle (RMs) of $w_0$ = 5. FRET from tryptophan to acrylodan in the model cavity was applied to confirm structural integrity of the cavity at various temperatures. The steady-state fluorescence spectra of AC in RMs of $w_0$ = 5 are presented in Fig. 5A. The [water]/[surfactant] ratio ($w_0$) was carefully chosen in our experiment. In one of our earlier studies, we have established that at $w_0$ = 5, the effect of temperature on the size of the RMs is little or insignificant [23]. In addition, we noticed that the non-radiative twisted intramolecular charge transfer [39] feasibility of AC in RMs of $w_0$ = 5 is minimum in

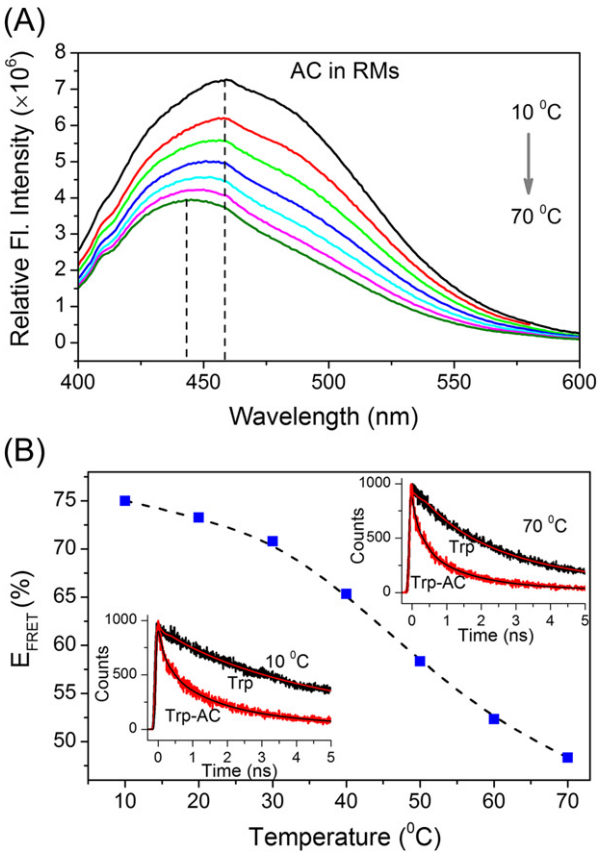


**Fig. 5.** (A) Represents the steady-state emission spectrum of acrylodan (AC) in AOT reverse micelle at various temperatures. Acrylodan emission is blue shifted and quenched with increase of temperature. (B) The energy transfer efficiency from tryptophan to acrylodan at various temperatures was estimated as represented in the figure. The dotted line is the guide to the eye. The inset figures represent the lifetime quenching of tryptophan in RMs in presence of acrylodan at two different temperatures. Tryptophan was excited at 299 nm and emission was collected at 350 nm.

**Table 3**
Fluorescence anisotropy decays, Wobbling-in-Cone data, microviscosity around the probe and energy barrier for viscous flow of acrylodan in ESA and in AOT RMs at different temperature values.

| Temperature (°C) | $\tau_{slow}$ (ns) | $\tau_{fast}$ (ns) | $\tau_{rot}$ (ns) | $\theta_W$ (deg) | $D_W \times 10^8$ (s$^{-1}$) | $\eta_m$ (cP) | $E_n$ (kcal mol$^{-1}$) |
|---|---|---|---|---|---|---|---|
| Acrylodan in ESA | | | | | | | 1.90 ± 0.2 |
| 10 | 60 (97%) | 0.53 (03%) | 58.33 | 7.8 | 0.10 | 8.38 | |
| 20 | 55 (95%) | 0.49 (05%) | 52.50 | 10.1 | 0.18 | 8.09 | |
| 30 | 42 (96%) | 0.41 (04%) | 40.62 | 8.5 | 0.15 | 6.97 | |
| 40 | 40 (96%) | 0.38 (04%) | 39.12 | 6.9 | 0.11 | 6.71 | |
| 50 | 36 (97%) | 0.30 (03%) | 35.21 | 6.9 | 0.14 | 5.41 | |
| 60 | 29(98%) | 0.11 (02%) | 28.42 | 6.6 | 0.35 | 2.04 | |
| 70 | 15 (94%) | 0.05 (04%) | 14.44 | 9.0 | 1.44 | 0.95 | |
| Acrylodan in AOT RMs | | | | | | | 2.05 ± 0.2 |
| 10 | 22 (67%) | 0.67 (33%) | 14.96 | 29.1 | 0.99 | 10.28 | |
| 20 | 20 (65%) | 0.60 (35%) | 13.21 | 30.1 | 1.18 | 9.33 | |
| 30 | 18 (64%) | 0.53 (36%) | 11.71 | 30.6 | 1.37 | 8.63 | |
| 40 | 16 (63%) | 0.40 (37%) | 10.23 | 31.2 | 1.87 | 7.69 | |
| 50 | 15 (62%) | 0.33 (28%) | 9.42 | 31.7 | 2.34 | 6.32 | |
| 60 | 13 (61%) | 0.28 (39%) | 8.04 | 32.2 | 2.84 | 5.58 | |
| 70 | 12 (61%) | 0.23 (39%) | 7.41 | 32.2 | 3.46 | 4.75 | |

comparison to higher $w_0$ values. As evident from Fig. 5A with increase in temperature, the relative intensity of acrylodan decreases and the emission spectrum is blue shifted. Inset of Fig. 5B represents the lifetime of tryptophan in reverse micelle in presence and in absence of acrylodan at various temperatures. In presence of acrylodan, the lifetime of tryptophan is significantly quenched due to FRET. The temperature dependency of the energy transfer process is represented in Fig. 5B. The lifetime traces of tryptophan in absence and in presence of acrylodan for two different temperatures (10 °C and 70 °C) are shown in the insets of Fig. 5B. The occurrence of FRET confirms the coexistence of tryptophan and acrylodan within AOT reverse micelle in our experimental temperature window. In order to understand the possible distribution of the acceptor molecules from the donor in the systems (protein and RMs), we have fitted the fluorescence transients of the donor in absence and presence of acceptor following equations (5) and (6) and are shown in Fig. 6. As shown in Fig. 6, at 10 °C, the half width (hw) of the distance distribution functions are 2 Å and 2.5 Å for protein (Fig. 6A and B) and RMs (Fig. 6C and D) respectively. The observed narrow distribution in the donor acceptor distance in the studied system may indicate their dynamical flexibility.

The estimated energy transfer efficiencies at various temperatures are plotted in Fig. 5B. As evident from the figure, energy transfer rate remains almost same up to 30 °C. With further increase of temperature, the energy transfer efficiency gradually decreases. The lifetime decay constants of tryptophan in RMs under various temperatures are tabulated in Table 1. As evident from the energy transfer studies, the probe acrylodan resides within the interior of reverse micelle (Fig. 1), which offers a unique opportunity to study the water dynamics of nano-size water pool inside the reverse micelle using the probe. Fig. 7A depicts the constructed TRES of acrylodan in RMs at 10 °C and 70 °C respectively. It is

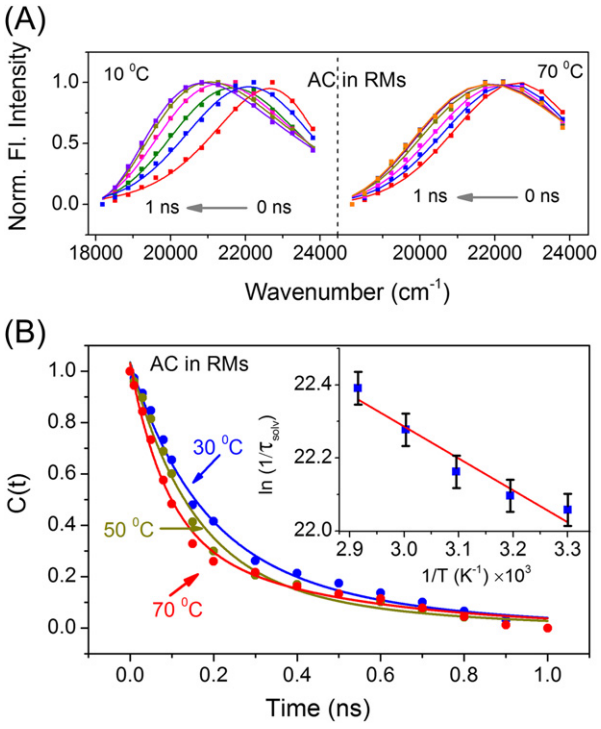


**Fig. 7.** (A) Depicts the constructed TRES for acrylodan in AOT reverse micelle at lower and higher temperatures. (B) Solvation correlation decay profiles of acrylodan in RMs are plotted for various temperatures. When the temperature was increased from 10 to 30 °C, insignificant change in $C(t)$ was observed. Inset shows the plot of $1/\tau_{solv}$ against $1/T$ (the solid line is a fitting to the Arrhenius equation with 1% error bar).

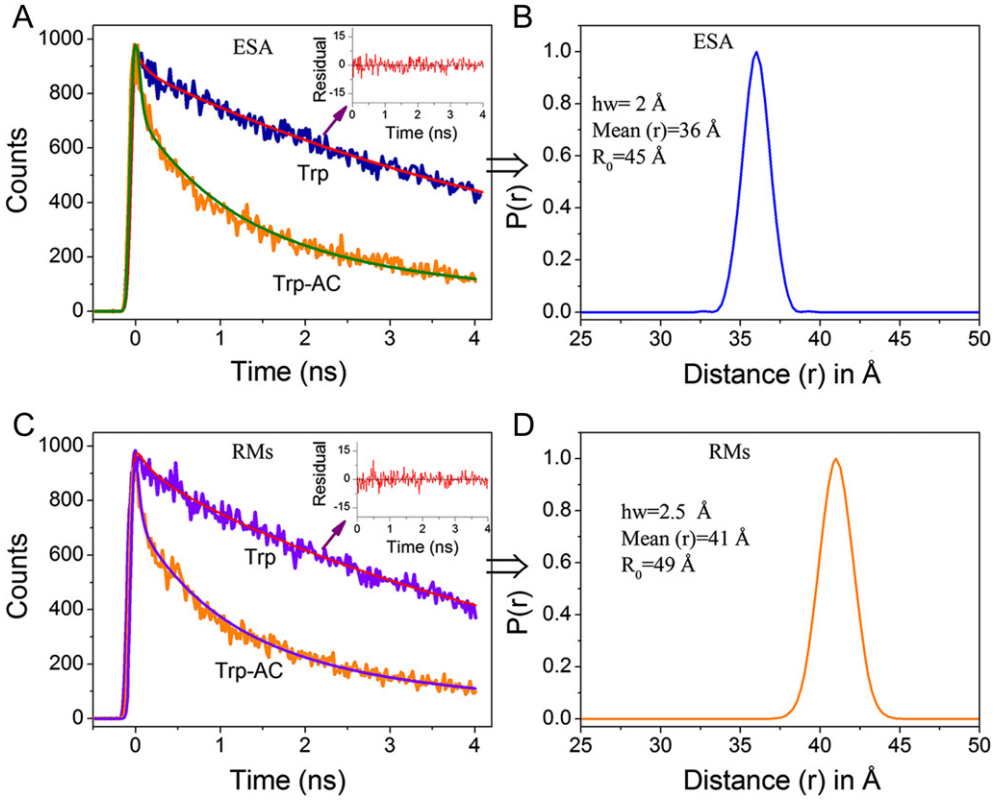


**Fig. 6.** (A) and (C) depict the fitting of time-resolved lifetime traces considering the distance distribution between donor and acceptor in ESA and RMs respectively. The inset shows the residual of the fitting. (B) and (D) show the probability of distance distribution ($P(r)$) with respect to mean distance.

evident from the figure that with increase of temperature, the net spectral shift decreases. The solvation correlation decay function, $C(t)$, of acrylodan was estimated for a temperature range of 10–70 °C and are represented in Fig. 7B. It has to be noted that, the temperature dependent solvation correlation decay function of acrylodan in RMs follows a different course than that in the protein. When the temperature is raised from 10 °C to 30 °C, little or insignificant change in the $C(t)$ was observed. After 30 °C, with further increase of temperature, the solvation correlation decay function becomes faster as elaborated in Fig. 7B. The corresponding solvation correlation decay constants at various temperatures are tabulated in Table 2. Inset of Fig. 7B represents the Arrhenius plot of activation energy barrier model. The slope of the plot of $\ln(1/\tau_{solv})$vs $1/T$ yielded a value of activation energy of $1.70 \pm 0.2$ kcal mol$^{-1}$. The result indicates that AC is located in the hydration shell at the interior of the RMs and solvation relaxation of AC essentially involves the transition between interfacially bound waters to quasi-bound state [20]. Insignificant change of $C(t)$ in the temperature region of 10–30 °C indicates the increase in temperature does not perturb the relaxation dynamics of water molecules inside the RMs in the temperature range.

Fig. 8A represents anisotropy decay plot of acrylodan in RMs at lower (10 °C) and elevated temperature (70 °C). The anisotropy experiments elucidate the rigidity of the probe molecules within RMs, and hence the water dynamics. At lower temperature (10 °C), the anisotropy consists of two decay components (22 ns (67%) and 0.67 ns (33%)). The slower 22 ns time component is due to the global motion of the RMs which is well corroborated with the estimated value using SED equation [29] considering the hydrodynamic radius of RMs (3.5 nm) for $w_0 = 5$ as reported in the literature [23]. At 70 °C, the anisotropy decay constant becomes 12 ns (61%) and 0.23 ns (39%). The corresponding time constants for the anisotropy decays are summarized in Table 3. Fig. 8B represents the change of diffusion coefficient for wobbling motion ($D_W$) value with increasing temperature. The diffusion coefficient ($D_W$) values are of the same order of magnitude as reported in one of our earlier work by Mitra et al. [23] for coumarin-500 in AOT RMs and increases with increasing temperatures. The corresponding semicone angles ($\theta_W$) experienced by the probe in different thermal regions are tabulated in Table 3. The observation is consistent with higher lability of the probe AC in the RMs at elevated temperature. Fig. 8C represents the plot of microviscosity, experienced by the probe at different temperatures. The energy barrier ($E_n$) for the viscous flow was estimated from the slope of the plot of $ln(\eta_m)$ against $1/T$ as described in equation (20). A good linear fit is obtained with a calculated $E_n$ value of $2.05 \pm 0.2$ kcal mol$^{-1}$. Reasonably good agreement between the energy barrier values ($E_n$ obtained from the rotational anisotropy study and $E_a$ value obtained from solvation dynamics study) is found.

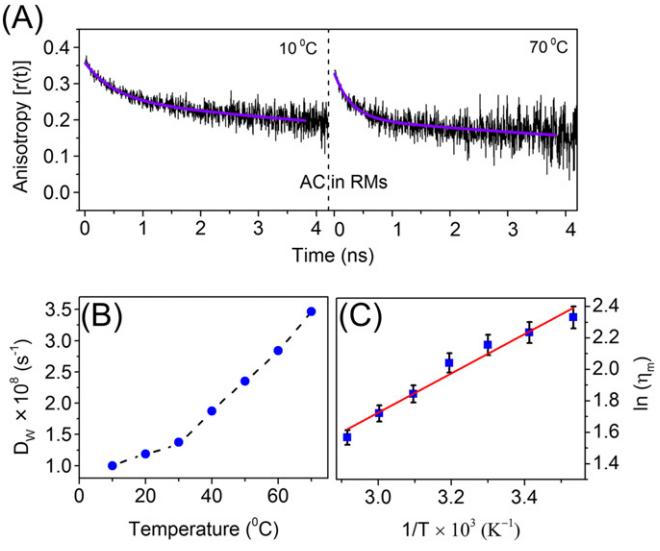


**Fig. 8.** (A) Temporal decays of rotational anisotropy of acrylodan in RMs at 10 °C and 70 °C are shown. (B) Diffusion coefficient for wobbling motion ($D_W$) of AC in AOT RMs at different temperatures. Dotted line is guide to eye. (C) Plot of $ln(\eta_m)$,$\eta_m$expressed in cP, against $1/T$ of AC in AOT RMs with a linear fit (5% error bar included).

## 4. Conclusion

In summary, we have carried out detail investigation of an important fluorescent probe acrylodan in biological and biomimetic cavities. The study provides some new insights about the cavity water dynamics for both biological and biomimetic systems. The estimated activation energy for water transition for both biological (ESA) and biomimetic (RMs) cavities using Arrhenius type activation energy model is similar and essentially indicates the water transition from bound to quasibound state. The rigidity of water molecules around Cys-34 of the protein cleft might have significant role in protein stability as well as crucial functional role in the ligand binding including an important anticancer drug doxorubicin. The persistency of the structural flexibility of the protein in the physiologically relevant temperature range (30–60 °C) as revealed from FRET and anisotropy studies is well justified from the perspective of protein activity. The considerable similarity of the dynamical properties of the water molecules in the protein cavity with that in the nano-droplets in the RMs is clearly revealed from our experiment. From the FRET studies, we have also observed a very narrow donor-acceptor distance distribution in the protein and RMs. The observation is important as a mammoth of theoretical (MD simulation in particular) and experimental understanding on the biomimetic RM-cavity is evident in the literature. Our experimental study is expected to have deep impact in the understanding of water relaxation/activity in hydrophobic cavity of protein interiors.

## Acknowledgments

SB thanks CSIR (India) for the research fellowships. We thank DST (India) for financial grants SR/SO/BB-15/2007.

## References

[1] D. Chandler, Interfaces and the driving force of hydrophobic assembly, Nature 437 (2005) 640–647.
[2] S. Matysiak, P.G. Debenedetti, P.J. Rossky, Role of hydrophobic hydration in protein stability: a 3D water-explicit protein model exhibiting cold and heat denaturation, J. Phys. Chem. B 116 (2012) 8095–8104.
[3] S. Somani, C.P. Chng, C.S. Verma, Hydration of a hydrophobic cavity and its functional role: a simulation study of human interleukin-1 beta, Proteins 67 (2007) 868–885.
[4] Y. Levy, J.N. Onuchic, Water mediation in protein folding and molecular recognition, Ann. Rev. Biophys. Biomol. Struct. 35 (2006) 389–415.
[5] N. Giovambattista, C.F. Lopez, P.J. Rossky, P.G. Debenedetti, Hydrophobicity of protein surfaces: separating geometry from chemistry, Proc. Natl. Acad. Sci. U. S. A. 105 (2008) 2274–2279.
[6] P. Rydberg, T.H. Rod, L. Olsen, U. Ryde, Dynamics of water molecules in the active-site cavity of human cytochromes P450, J. Phys. Chem. B 111 (2007) 5445–5457.
[7] B. Yu, M. Blaber, A.M. Gronenborn, G.M. Clore, D.L.D. Caspar, Disordered water within a hydrophobic protein cavity visualized by X-ray crystallography, Proc. Natl. Acad. Sci. U. S. A. 96 (1999) 103–108.
[8] C. Carey, Y.-K. Cheng, P.J. Rossky, Hydration structure of the α-chymotrypsin substrate binding pocket: the impact of constrained geometry, Chem. Phys. 258 (2000) 415–425.
[9] J.C. Rasaiah, S. Garde, G. Hummer, Water in nonpolar confinement: from nanotubes to proteins and beyond, Ann. Rev. Phys. Chem. 59 (2008) 713–740.

[10] F. Kratz, A. Warnecke, K. Scheuermann, C. Stockmar, J. Schwab, P. Lazar, P. Druckes, N. Esser, J. Drevs, D. Rognan, C. Bissantz, C. Hinderling, G. Folkers, I. Fichtner, C. Unger, Probing the cysteine-34 position of endogenous serum albumin with thiol-binding doxorubicin derivatives. Improved efficacy of an acid-sensitive doxorubicin derivative with specific albumin-binding properties compared to that of the parent compound, J. Med. Chem. 45 (2002) 5523–5533.
[11] J.K.A. Kamal, L. Zhao, A.H. Zewail, Ultrafast hydration dynamics in protein unfolding: human serum albumin, Proc. Natl. Acad. Sci. U. S. A. 101 (2004) 13411–13416.
[12] S.K. Pal, A.H. Zewail, Dynamics of water in biological recognition, Chem. Rev. 104 (2004) 2099–2123.
[13] A.J. Ryan, J. Ghuman, P.A. Zunszain, C.-w. Chung, S. Curry, Structural basis of binding of fluorescent, site-specific dansylated amino acids to human serum albumin, J. Struct. Biol. 174 (2011) 84–91.
[14] R.K. Mitra, S.S. Sinha, S.K. Pal, Hydration in protein folding: thermal unfolding/refolding of human serum albumin, Langmuir 23 (2007) 10224–10229.
[15] K. Flora, J.D. Brennan, G.A. Baker, M.A. Doody, F.V. Bright, Unfolding of acrylodan-labeled human serum albumin probed by steady-state and time-resolved fluorescence methods, Biophys. J. 75 (1998) 1084–1096.
[16] K. Bhattacharyya, Solvation dynamics and proton transfer in supramolecular assemblies, Acc. Chem. Res. 36 (2002) 95–101.
[17] R. Saha, S. Rakshit, R.K. Mitra, S.K. Pal, Microstructure, morphology, and ultrafast dynamics of a novel edible microemulsion, Langmuir 28 (2012) 8309–8317.
[18] D. Pant, N.E. Levinger, Polar solvation dynamics in nonionic reverse micelles and model polymer solutions, Langmuir 16 (2000) 10123–10130.
[19] S. Pal, S. Balasubramanian, B. Bagchi, Temperature dependence of water dynamics at an aqueous micellar surface: atomistic molecular dynamics simulation studies of a complex system, J. Chem. Phys. 117 (2002) 2852–2859.
[20] S. Balasubramanian, S. Pal, B. Bagchi, Hydrogen-bond dynamics near a micellar surface: origin of the universal slow relaxation at complex aqueous interfaces, Phys. Rev. Lett. 89 (2002) 115505–115508.
[21] J.R. Lakowicz, Principles of Fluorescence Spectroscopy, Kluwer Academic/Plenum, New York, 2006.
[22] M.L. Horng, J.A. Gardecki, A. Papazyan, M. Maroncelli, Subpicosecond measurements of polar solvation dynamics: coumarin 153 revisited, J. Phys. Chem. 99 (1995) 17311–17337.
[23] R.K. Mitra, S.S. Sinha, S.K. Pal, Temperature-dependent solvation dynamics of water in sodium bis(2-ethylhexyl)sulfosuccinate/isooctane reverse micelles, Langmuir 24 (2007) 49–56.
[24] K. Kinosita Jr., A. Ikegami, S. Kawato, On the wobbling-in-cone analysis of fluorescence anisotropy decay, Biophys. J. 37 (1982) 461–464.
[25] R. Saha, P.K. Verma, R.K. Mitra, S.K. Pal, Structural and dynamical characterization of unilamellar AOT vesicles in aqueous solutions and their efficacy as potential drug delivery vehicle, Colloids Surf. B 88 (2011) 345–353.
[26] B. Kalman, N. Clarke, L.B.A. Johansson, Dynamics of a new fluorescent probe, 2,5,8,11-tetra-tert-butylperylene in solution, cubic lyotropic liquid crystals, and model membranes, J. Phys. Chem. 93 (1989) 4608–4615.
[27] L.A. Philips, S.P. Webb, J.H. Clark, High-pressure studies of rotational reorientation dynamics: the role of dielectric friction, J. Chem. Phys. 83 (1985) 5810–5821.
[28] Y.H. Zhao, M.H. Abraham, A.M. Zissimos, Fast calculation of van der Waals volume as a sum of atomic and bond contributions and its application to drug compounds, J. Org. Chem. 68 (2003) 7368–7373.
[29] D. Lavalette, C. Tetreau, M. Tourbez, Y. Blouquit, Microscopic viscosity and rotational diffusion of proteins in a macromolecular environment, Biophys. J. 76 (1999) 2744–2751.
[30] G. Weber, F.J. Farris, Synthesis and spectral properties of a hydrophobic fluorescent probe: 6-propionyl-2-(dimethylamino)naphthalene, Biochemistry 18 (1979) 3075–3078.
[31] J. González-Jiménez, M. Cortijo, Resonance energy transfer between tryptophan-214 in human serum albumin and acrylodan, prodan, and promen, Protein J. 23 (2004) 351–355.
[32] M.A. Tricerri, A.K. Behling Agree, S.A. Sanchez, A. Jonas, Characterization of apolipoprotein a-I structure using a cysteine-specific fluorescence probe, Biochemistry 39 (2000) 14682–14691.
[33] N. Nandi, B. Bagchi, Dielectric relaxation of biological water, J. Phys. Chem. B 101 (1997) 10954–10961.
[34] R.K. Mitra, S.S. Sinha, S.K. Pal, Temperature-dependent hydration at micellar surface: activation energy barrier crossing model revisited, J. Phys. Chem. B 111 (2007) 7577–7583.
[35] S. Pal, S. Balasubramanian, B. Bagchi, Identity, energy, and environment of interfacial water molecules in a micellar solution, J. Phys. Chem. B 107 (2003) 5194–5202.
[36] P. Sen, S. Mukherjee, A. Halder, K. Bhattacharyya, Temperature dependence of solvation dynamics in a micelle. 4-Aminophthalimide in Triton X-100, Chem. Phys. Lett. 385 (2004) 357–361.
[37] R. Zana, Microviscosity of aqueous surfactant Micelles: effect of various parameters, J. Phys. Chem. B 103 (1999) 9117–9125.
[38] S.K. Pal, J. Peon, A.H. Zewail, Biological water at the protein surface: dynamical solvation probed directly with femtosecond resolution, Proc. Natl. Acad. Sci. U. S. A. 99 (2002) 1763–1768.
[39] T. Mondol, S. Batabyal, A. Mazumder, S. Roy, S.K. Pal, Recognition of different DNA sequences by a DNA-binding protein alters protein dynamics differentially, FEBS Lett. 586 (2012) 258–262.